SAND83-0779C

HYDROGEN GE..TRATION DURING A CORE MELT-COOLANT INTERACTION

M. L. Corradini
University of Wisconsin
Madison, WI

D. E. Mitchell and N. A. Evans
Sandia National Laboratories
Albuquerque, NM

If a reactor accident leads to core melt, interaction of this material with coolant can produce hydrogen by steam oxidation of the metallic content of the melt. In this paper we present experimental results for hydrogen generation from both explosive and non-explosive melt-coolant interactions, using either iron-alumina or corium A + R as the melt simulant. Use of a simple model gives predictions for hydrogen generation rates that are in reasonable agreement with the experimental results.

INTRODUCTION

Given the absence of adequate cooling water to the core of a light-water reactor (LWR), the fission product decay heat would eventually cause the reactor fuel and cladding to melt. This could lead to slumping of the molten core materials into the lower plenum of the reactor vessel, possibly followed by failure of the vessel wall and pouring of the molten materials into the reactor cavity. Recent analyses (1-5) have indicated that residual water is likely to be present both in the lower plenum and in the reactor cavity. Therefore, when the molten core materials enter either region, there is a strong probability of the melt contacting water. The contact of molten fuel with water can result in either explosive or non-explosive events, both of which can produce steam and hydrogen at rapid rates. The final size of the debris also depends on the type of interaction.

In this paper we are concerned principally with the generation of hydrogen from a core-melt/coolant interaction (CMCI). To our knowledge this is the first time experimental data have been reported on hydrogen production from a CMCI at a scale of 20 kg. Past research into melt-water reactions (e.g. 6,7) has dealt primarily with the correlation of reaction kinetics of solid metal oxidation, although some data on the molten metal oxidation were collected. The CMCI is unique in this respect in that both molten metal and solid metal oxidation can occur.

There are several ways that metal can be oxidized during a severe accident in a LWR. For metal oxidation producing hydrogen during a CMCI, the distinguishing features are that the metal is initially in a molten state, and the melt pours or falls into a water pool. The mode of heat transfer and the level of oxidation depend on the details of the mixing and fragmentation processes. These processes can be distinguished by the following features:

(1) A 'free-contacting' mode where the melt has been poured or injected into a coolant pool, falls freely under the influence of gravity, and mixes with the coolant. In this case the melt-coolant geometry is one of melt drops, of various sizes, in film boiling surrounded by the liquid coolant.

(2) A steam explosion could occur while the melt is falling through the water pool. In this case the melt would be fragmented into much finer debris sizes and be ejected into the surrounding atmosphere.

(3) If a steam explosion does not occur after the melt mixes with the water, then the melt will settle on the chamber base and reagglomerate as a stratified molten pool and possibly be slowly quenched by the water layer on top of it, or remelt.

We have performed a series of scoping experiments using melt simulant materials and water to investigate hydrogen production during a CMCI. In conjunction with these tests, supporting analysis has been performed to calculate the amount of hydrogen generated during these processes. We first discuss the experimental apparatus and the tests performed, and then present our calculations for hydrogen production in these tests.

EXPERIMENTAL APPARATUS

The FITS-C experiments for investigating hydrogen production were conducted in a closed chamber (Fig. 1). Earlier tests outside the chamber were performed to develop instrumentation and melt delivery techniques; the in-chamber experiments allowed for more detailed measurements (temperature, pressure histories, hydrogen concentrations) and the collection of the explosion debris (see Ref. 8 for further details of the apparatus).

The water interaction chambers used were designed in the form of rectangular parallelopipeds, with square cross-sectional areas and open tops. These were fabricated from clear, 6.3 mm thick plexiglass stock in sizes to produce initial water-to-melt mass ratios of 6:1 to 13:1.

*This work was performed at Sandia National Laboratories and supported by the U. S. Department of Energy under Contract number DE-AC04-76DP00789 for U. S. Nuclear Regulatory Commission, Office of Research.

The melt used in these experiments was prepared by a metallothermic (thermite) reaction. The resulting melt consisted of either iron-alumina (55 w/o-iron, 45 w/o-alumina) or corium (corium-A+R: 70 w/o - UO_2/ZrO_2, 30 w/o-stainless steel) at a theoretical (maximum) temperature of 3100 K. This corresponds to an internal energy content of 3.3 MJ/kg for iron-alumina and 1.8 MJ/kg for the corium. Calorimetry tests indicated that the actual fuel internal energy was about 90% of this value. This suggests an entry temperature into the water pool $\leq$2800 K; this value is in agreement with optical pyrometer measurements made in a few tests of the surface of the melt mass. Iron-alumina was used in these tests because it is an inexpensive high-temperature simulant for the more prototypic melt (corium), and we wished to determine any differences in the oxidation behavior of the two materials.

Water from the local water supply was used as the coolant. No special treatment, such as degassing or deionizing, was done. Water temperature was not controlled for the majority of the experiments, and was between 309 and 319 K.

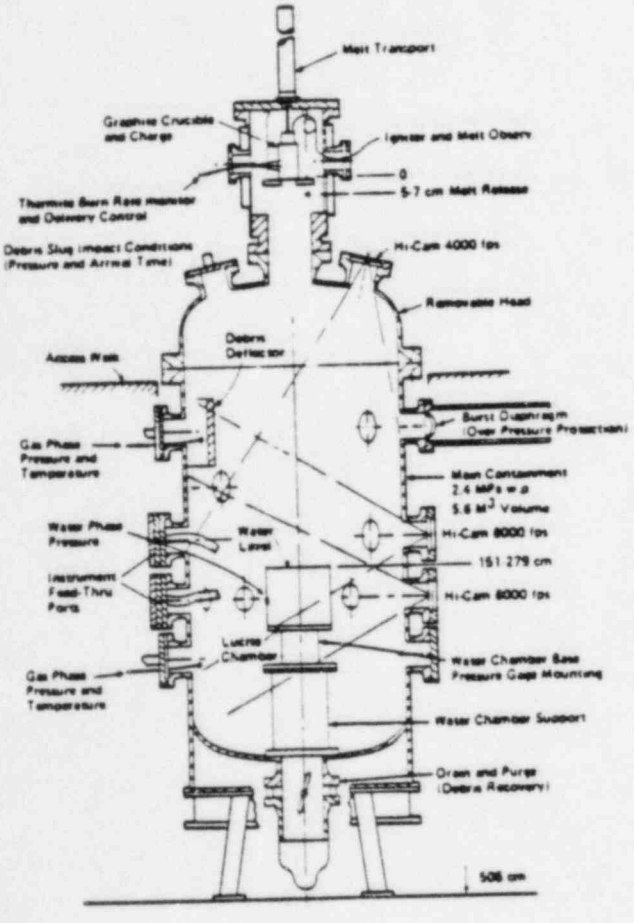

Figure 1. Fits Test Chamber

The experiments were instrumented with pressure transducers: in the water chamber base and side walls to measure water phase pressure; in the chamber upper head to study debris slug characteristics; and in the FITS chamber side wall ports to measure the gas phase pressure. Melt delivery was initiated automatically through the use of probes in the crucible that sensed when the thermite reaction was complete. Melt entry time was measured by photodiodes 2.5 cm above the water surface; the shape and velocity of the melt at water impact and during mixing were recorded by high-speed cameras. Debris recovered from the experiments was characterized by sieving using sieve sizes ranging from 38 μm to 25 mm.

EXPERIMENTAL RESULTS

Five tests were performed in the FITS chamber (Table 1) with nitrogen used as an inert cover gas (99 v/o) in order to obtain post-test samples of the unreacted hydrogen produced by metal oxidation. Analysis was performed using gas chromatography. Gas and water phase pressures and temperatures were measured during the tests and post-test debris was collected. An iron-alumina melt was used in FITS-1C to repeat the initial conditions used in an earlier test, FITS-2B (except that FITS-2B used air as a cover gas which prevented hydrogen measurements because combustion occurred). Following this, FITS-2C and -3C were conducted with corium A+R. Of the last two experiments in the series only one (FITS-5C) was successful, and used iron-alumina with a high system pressure, P_∞ = 0.5 MPa; the water temperature was increased to maintain the subcooling at $\Delta T_{sub} \cong$ 70 K, as in FITS-1C to -3C.

Preliminary analysis of the photographic data and available pressure records indicated that the results were similar to those observed in the FITS-B experimental series (9). As an example, consider the behavior of FITS-1C (see Figs. 2 to 5). A coherent melt mass of 17 kg was delivered into 110 kg of water at an entry velocity of approximately 5 m/s (see ref. 8 and 9 for details of the delivery system). Approximately 130 msec after melt entry, a single, spontaneous steam explosion was triggered at the top surface of the melt-coolant mixture. This was quite similar to the result obtained in the FITS-2B experiment previously mentioned. The melt entered the water pool and dispersed in the shape of a paraboloid as in previous tests. Individual molten droplets could be distinguished at the periphery of the melt-coolant mixture with diameters in the range of 10-20 mm. Gas phase pressure transducers in FITS-1C measured a peak explosion pressure (see Fig. 2) in the FITS chamber of 0.36 MPa with a quasi-static pressure of 0.25 MPa over the first few seconds.

The debris from the explosion in FITS-1C was collected and separated into thirty subsections by sieving. The debris exhibited a somewhat bimodal distribution (Figs. 4 and 5) with the majority of particles in the range of 100 to 300 μm. The mass average diameter for the debris was approximately 300 μm, while the Sauter mean diameter was 225 μm (the Sauter mean diameter is that size which represents the correct debris volume-to-surface-area ratio for a collection of particles). This debris distribution can be compared to that obtained for FITS-2C (Figs. 4 and 5) which involved 17 kg

Table 1 FITS-C EXPERIMENTS - INITIAL CONDITIONS AND RESULTS

Test	Melt Mass (Type)	Coolant to Melt Mass Ratio	Water Temp (K)	Chamber Dimensions	Gas	Gas Pressure (MPa)	Results
FITS-1C	17kg Iron-alumina*	6.6	298	0.61 m square and 0.3 m deep	N_2	0.083	Spontaneous surface triggered explosion 130 mm after melt entry Results similar to FITS-2B.
FITS-2C	17.0 kg Corium-A+R*	13.0	295	0.61 m square and 0.61 m deep	N_2	0.083	Spontaneous surface triggered explosion 30 ms after melt entry. Weak spontaneous base-triggered explosion 150 ms after entry.
FITS-3	11.5 kg Corium-A+R	9.8	299	0.53 m square and 0.4 m deep	N_2	0.083	No explosion or trigger sites observed. Melt dispersed at entry (entered as a series of 1-2 cm dia. drops).
FITS-4	19 kg	5.9	300	0.61 m square	N_2	0.59	No spontaneous explosion. External trigger failed to fire. Gas samples lost. Test to be repeated as FITS-5C.
FITS-5C	19.5 kg	5.8	298	0.61 m square	N_2	0.58	No spontaneous explosion, dispersed delivery. No trigger signal. Gas samples obtained.

*Iron-Alumina: 45 w/o - Al_2O_3, 55 w/o - Fe
Corium-A+R: 70 w/o - UO_2/ZrO_2, 30 w/o - stainless steel

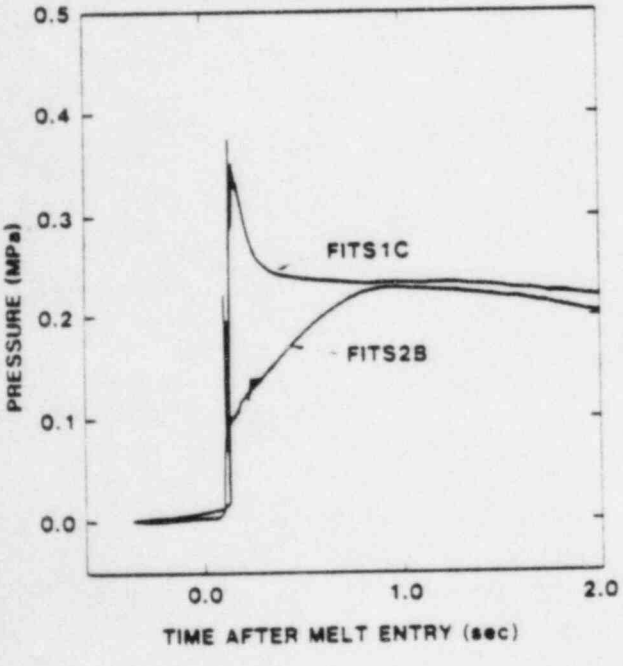

Figure 2. Comparison of Chamber Pressure Records (Early Time)

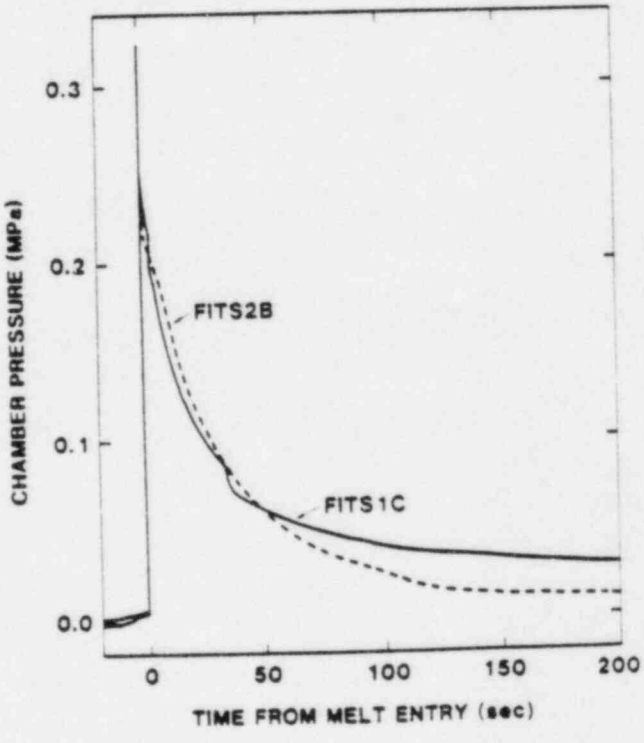

Figure 3. Comparison of Chamber Pressure Records (Late Time)

of corium-A+R dropped into water. FITS-2C resulted in an early, spontaneous, surface trigger 30 msec after fuel melt entry, followed by a second weak (spontaneous) base-triggered explosion 150 msec after entry. These results were qualitatively similar to three FITSB experiments which involved multiple explosions. In this test it would appear that the explosion conversion ratio was lower than in FITS-1C, as shown by the relatively coarser debris sizes: the mass average diameter was 1000 um and Sauter mean diameter was 750 um.

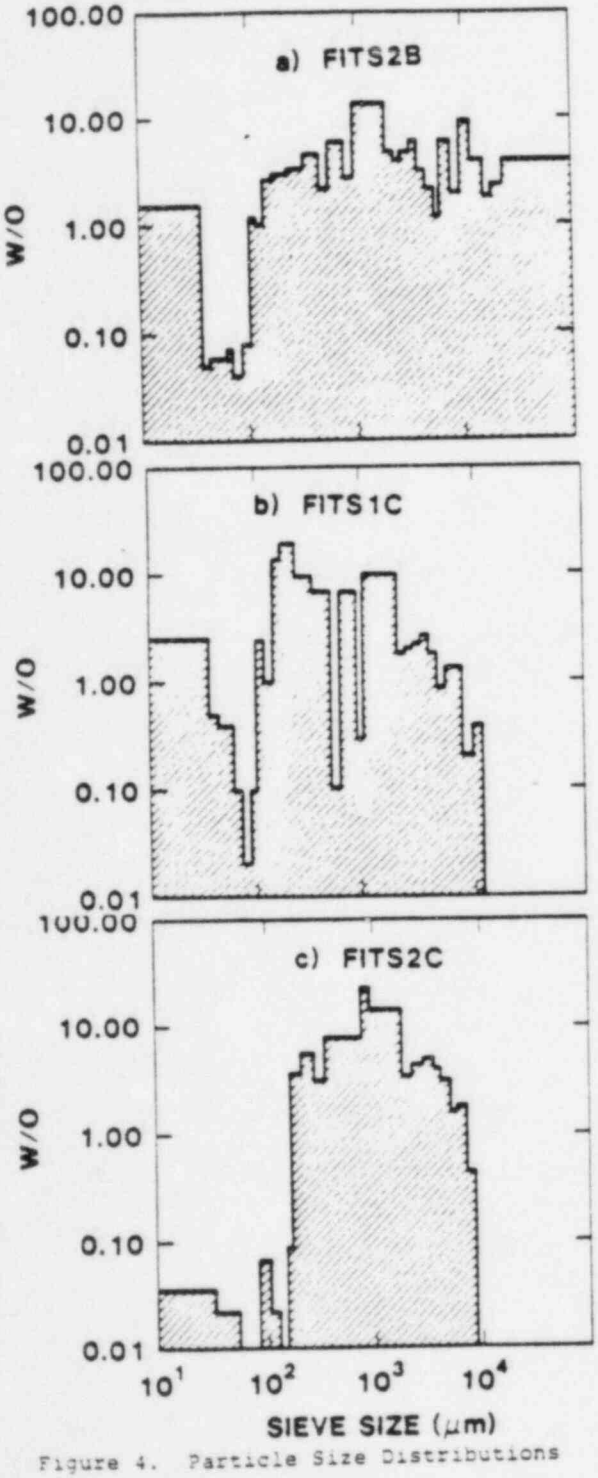

Figure 4. Particle Size Distributions

The explosive behavior of FITS-1C and -2C should be contrasted with the non-explosive behavior of FITS-3C and -5C. In FITS-3C the corium-A+R melt entered the water pool and mixed with the surrounding coolant in an array of 10-20 mm particles at the mixture periphery. However, as it settled to the water chamber base, no spontaneous triggers were observed and the molten particles reagglomerated into a coherent mass on the chamber base and slowly quenched. Similar behavior was observed for FITS-5C; as noted above, FITS-4C did not result in a successful melt delivery.

The four successful FITS-C tests show that the amount of hydrogen generated depends strongly on the type of melt-coolant interaction, and the sizes of the particles produced. The amount of hydrogen produced ranged from a few grams to about one hundred grams. The presence of a spontaneously triggered steam explosion had the greatest effect on the amount of hydrogen produced. In FITS-1C and -2C the enhanced melt surface area contributed to the larger amounts of hydrogen produced. Pre- and post-test gas samples from each test were analyzed using a gas chromatograph. Based on the results of the gas analysis, and knowing the approximate mass of the metallic phase in the melt, we estimated the percentage of melt that reacted to produce the hydrogen. The results are given in Table 2, where the higher percentage value assumes FeO was formed, and the lower value assumes Fe_2O_3 was formed.

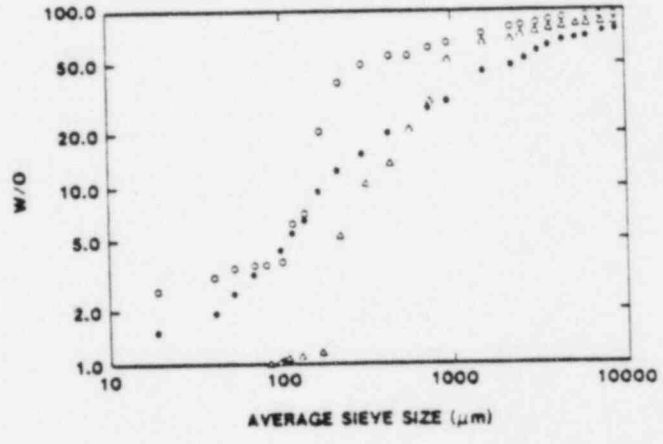

Figure 5. Cumulative Debris Size Distributions

● Fits 2B
○ Fits 1C
Δ Fits 2C

ANALYSIS OF EXPERIMENTS

The amount of hydrogen generated during a CMCI is the product of two factors: the first is the chemical kinetic rate of metal oxidation per unit surface area as the melt cools and solidifies, and the second is the available melt surface area that evolves during the CMCI. For the purpose of analyzing hydrogen generation, the features of the FITS-C experiments can be classified as follows: 'free contact' fuel-coolant mixing; a steam explosion; and a reagglomerated melt-coolant state. Let us first look at the rate of chemical reaction, followed by the surface area available, and then estimate the amount of hydrogen generated.

TABLE 2 - Hydrogen Generation Results

Test	Percent of Metal Reacted	Hydrogen Mass Generated (gm) from FITS-C Data	Hydrogen Mass Generated (GM) by Calculation
FITS-1C	22-33%*	110	105-110
FITS-2C	18-26%	48	35-40
FITS-3C	4-6%	7.5	5
FITS-5C	9-13%	49	45

*The first value assumes formation of Fe_2O_3 and the second value assumes formation of FeO.

Rate of Chemical Oxidation

Metal oxidation is practically limited by mass transfer in the gas and liquid (or solid) phases near the melt surface (10, 11). In the gas phase, steam must diffuse to the melt surface through the hydrogen which is being generated. In the liquid phase in the absence of bulk convection, if the oxide formed remains a liquid around the molten metal drop, the oxygen atoms must diffuse to the unreacted metal through the layer being built up; the same process is true for the case where the oxide is a solid shell or crust atop the molten metal surface. These two rate-limiting processes are considered in the prediction of the hydrogen generation rate.

The first mass transfer resistance is the diffusion of the steam through the gas to the metal surface. Following past work in this area (12), the governing mass transfer equation can be written in a somewhat general form for equimolar counter-diffusion of two perfect gases as

$$\frac{dN_H}{dt} = A \frac{D_H}{R_o T_v} \frac{dP_H}{dn} \qquad (1)$$

where $\frac{dN_H}{dt}$ is the molar rate of hydrogen diffusion in steam (mole/s),
D_H is the diffusion coefficient for hydrogen and steam,
R_o is the universal gas constant,
P_H is the hydrogen partial pressure,
T_v is the gas-vapor temperature,
n is the outward directed normal direction,
A is the surface area: $4\pi r^2$ for a droplet or L^2 for a plane.

One can integrate this equation with respect to n for a certain geometry (planar or spherical) if one assumes that the diffusion coefficient is a constant stemming from the total pressure in the gas-vapor phase and the mean film temperature, T_v (equal to the average of the water saturation temperature T_{sat}, and the melt surface temperature, T_m).

The second mass transfer resistance is the diffusion of oxygen atoms through the melt oxide (solid or liquid) to the unreacted metal. This diffusion process is quite complex; for example, for solids, hydrogen generation rates are empirically correlated from test data (6,7) under the boundary conditions that an excess of steam is present, and the solid metal oxide film or crust resists further mass transfer. For steel, the rate of reaction is given by a parabolic kinetics expression

$$\frac{d}{dt}(W^2) = 3.8\ (10^3) \exp \frac{84300}{R_o T_v} \qquad (2)$$

where W is the cumulative mass of hydrogen in kg/m^2, and R_o is given here specifically in cal/gmole K. For a liquid oxide the process is even more complex because the oxide may be miscible in the metal or the molten metal, and could become mechanically mixed by internal currents caused by temperature or relative velocity.

We believe that, when the oxide is liquid, these two latter effects cause the primary mass transfer resistance to be in the gas-vapor film. When the oxide is a solid film or crust we can utilize the empirical parabolic kinetic models derived from experimental data; this then becomes the dominant mass transfer resistance.

Hydrogen Generation During Melt-Coolant Mixing

When the melt first enters the water pool in the FITS tests it disperses and mixes with the water as it breaks apart into smaller molten droplets which are surrounded by a vapor film in a continuum of liquid coolant. Past work in melt-coolant mixing (10,12) indicates that the molten droplets decrease in size with time to some lower limit determined by steam generation rates and fluidization criteria. Currently, a simple dynamic mixing model has been developed (13) which describes the transient mixing process of melt and water. We have used this model to predict the amount of hydrogen generated during this 'free-contact' fall phase of fuel melt in coolant. To illustrate the model we present a simplified formulation here.

If steam diffusion through the gas-vapor film separating melt and coolant is considered by the reasoning above to be the dominant mass transfer resistance and the process is assumed to be quasi-steady, we can rewrite Eq. 1 in spherical coordinates ($A \equiv 4\pi r^2$, $n \equiv r$) and integrate across the gas-vapor film thickness. The resulting equation is

$$\frac{dN_H}{dt} = \frac{4\pi D_H \Delta P_H}{R_o T_v} \left(\frac{1}{R_m} - \frac{1}{R_m + \delta} \right)^{-1} \qquad (3)$$

where ΔP_H is the difference in partial pressure at the melt and coolant liquid surfaces, R_m is the melt droplet radius, and is the gas-vapor film thickness. Based on the dynamic mixing model (13), R_m is calculated to vary according to

$$D_m = D_{m_o} \exp(-T^*) \qquad (4)$$

where $D_{m_o} = 2R_{m_o}$ is the original melt diameter, and T^* is the dimensionless time after the melt enters the water:

$$T^+ \equiv \frac{t_v}{D_{m_o}} v_{m_o} \left(\frac{\rho_c}{\rho_m}\right)^{1/2} \quad (5)$$

where t_v is time
v_{m_o} is the entry velocity, and
ρ_c, ρ_m is the density of coolant, c, and melt, m. The vapor film thickness in film boiling can be derived quite simply from first principles if one assumes a laminar vapor film flow, resulting in

$$\delta = 2\left[\frac{k_v D_m \mu_v (T_m - T_{sat})}{\rho_v(\rho_c - \rho_v) g\, i_{fg}}\right]^{1/4} \quad (6)$$

where k_v and μ_v are the vapor thermal conductivity and viscosity, respectively, g is the gravitational acceleration, and i_{fg} is the latent heat of vaporization.

Eqs. 3-6 give the rate of hydrogen generation per droplet. The total generation rate is found by multiplying the rate for one droplet by the total number of droplets

$$N_{TOT} = \frac{6m_m}{\rho_m \pi D_m^3} \quad (7)$$

where m_m is the fuel melt mass. One should note that there is some uncertainty in N_{TOT}; one could assume the melt is homogeneous and the mass is the metallic mass at the mixture density or, conversely, the melt is heterogeneous with melt droplets separate from the oxide or completely covering the oxide drops. This introduces some range into the actual number of metallic droplets and the exposed surface area.

If one now combines the resulting Eqs. 3-7 and integrates over the observed time, t_{fall}, it takes the melt to fall through the water pool (or to an explosion trigger site), the resultant simplified expression becomes

$$N_H = \left(\frac{D_H}{R_o T_v}\right)\left(\frac{6m_m \Delta p_H}{\rho_m D_{m_o} \delta}\right)\left[\frac{\exp(-T^+(t_{fall} - 1)}{T^+}\right] t_{fall} \quad (8)$$

where we have assumed, for the sake of illustration, that the melt temperature is constant and $\delta \ll R_m$.

This calculation also includes use of the dynamic mixing model. Because the water depth was so small in the FITSC series (0.3m), one can calculate that only a few tenths of a gram of hydrogen are generated during the fall of the melt in the pool. This result is consistent with the observation that the melt enters as a somewhat coherent mass and does not mix significantly in the shallow depth of water, causing the exposed surface area to be low. This suggests that the steam explosion or the stratified melt quenching process produces the majority of hydrogen.

Hydrogen Generation During a Steam Explosion

For the steam explosion the geometry is quite similar to mixing, since an array of fuel melt droplets is produced. However, now the melt droplets are carried along as finely fragmented molten melt particles and are quenched in the expanding high pressure steam which is generated. Therefore, one can use Eq. 1 again for the mass transfer rate when the fuel is molten, but now the characteristic length is the fuel melt diameter. Integrating Eq. 1 produces:

$$\frac{dN_H}{dt} = 2\pi D_m^2 \left(\frac{D_H}{R_o T_v}\right)\frac{\Delta p_H}{D_m} \quad (9)$$

When the melt surface solidifies the mass transfer resistance is dominated by the solidified oxide film or crust, and the weight gain is given by an empirical parabolic rate equation like Eq. 2 for steel. The fuel melt droplet diameter would now be given by the post-explosion fragment size. Also, the pressure in the gas-vapor phase would begin at a high value and decrease with time; however, because the diffusion coefficient, D_H, is inversely proportional to pressure, this variation counterbalances the increase in Δp_H.

The fuel melt temperature would decrease with time as the melt quenches; this would be the major transient effect because, when the fuel is molten, the diffusion coefficient, D_H, is approximately proportional to $T_v^{1.5}$. If we divide the fuel melt quench process at the point when the oxide crust solidifies, T_{sol}, (1800K for iron oxide) then we can calculate the quench time to T_{sol} for steam-diffusion-controlled mass transfer. By a simple energy balance for a fuel droplet we obtain

$$\rho_m \frac{\pi}{6} D_m^3 c_m \frac{dT_m}{dt} = \frac{-2k_v}{D_m} \pi D_m^2 (T_m - T_\infty) \quad (10)$$

where c_m is melt specific heat and T_∞ is the ambient temperature, and we have assumed that the fuel behaves as a lumped volume (Biot number $\ll 0.1$). We have also used a Nusselt number of two, indicating that, for these small fuel melt diameters (200 μm), the droplet moves at the same velocity as the gas-vapor phase. We have also assumed that the energy produced from the exothermic iron oxidation is negligible compared to the heat loss rate. The time to reach the oxide solidification temperature is given by integrating eq. (10):

$$t_{sol} = \frac{1}{C_o} \ln \frac{T_m - T_\infty}{T_{sol} - T_\infty} \quad (11)$$

$$\text{where } C_o = \frac{12k_v}{\rho_m D_m^2 c_m} \quad (12)$$

For FITS-1C and 2C this time is on the order of 50 to 100 msec, which is much smaller than the time to the quasi-steady pressure when the melt debris has

settled after the explosion; this suggests we can use this characteristic time to compute hydrogen generation after the explosion. Combining Eqs. 7, 9, and 11 and integrating from the time of the explosion to t_{sol} gives

$$N_H = \frac{4\pi D_m^2}{3}\left(\frac{D_H}{R_o T_v}\right)\frac{\Delta P_H}{D_m}\left[\frac{2T_\infty + \Delta T_m(1-C_o t_{sol})}{T_\infty + T_m}\right]^{3/2} x\left(\frac{T_m + T_\infty}{T_m C_o}\right), \text{ where } \Delta T_m = T_m - T_\infty. \quad (13)$$

After the metal oxide surface has begun to solidify, we can use Eq. 2 with Eq. 7 to find the amount of hydrogen generated as the melt continues to cool. Practically, after the oxide surface of the melt has solidified, the rate of hydrogen generation decreases so rapidly that Eq. 13 approximately provides the total amount of hydrogen produced during the explosion. Table 2 gives the results of the calculation for FITS-1C and 2C where we have used the FITS Sauter mean diameter for D_m. The lower value in the Table assumes that the metal phase is separate from the oxide as individual droplets. This assumption is based on the concept that the melt is heterogeneous. If the melt is a homogeneous mixture, then the actual value is bounded by the higher figure. The agreement with the actual experimental value is surprisingly good, suggesting this simple approach is valid for an order-of-magnitude experimental data analysis.

Hydrogen Generation During Stratified Melt Quenching

For the case where the melt has fallen through the water pool and reagglomerated on the chamber base, the melt will be oxidized by the water layer above it. The mass transfer resistance when the metal is molten is given by Eq. 1 in a linear form ($A = L^2$, L = chamber width and $n = x$), with the integration taken over the vapor film thickness, δ, separating the melt and the water:

$$\frac{dN_H}{dt} = A\frac{D_H}{R_o T_v}\frac{\Delta P_H}{\delta} \quad (14)$$

where δ is now given by the film boiling thickness for a large flat plate:

$$\delta = 0.7\left[\frac{k_v \lambda_c \mu_v (T_m - T_{sat})}{\rho_v(\rho_c - \rho_v) g\, i_{fg}}\right]^{1/4} \quad (15)$$

In Eq. 15, λ_c is the critical Taylor wavelength given by

$$\lambda_c = 2\pi\sqrt{\frac{\sigma_c}{(\rho_c - \rho_v)g}} \quad (16)$$

where σ_c is the water surface tension. Again, when the metal oxide begins to solidify, it will be necessary to use Eq. 2.

As in the case of the steam explosion, the melt will cool, and the temperature decrease will affect the diffusion coefficient, causing it to decrease; this will reduce the rate of hydrogen production while the metal is molten. The time to solidification of this melt layer is given by an energy balance similar to Eq. 10 except that in this case, the melt is stratified as a layer.

$$\text{Hence } t_{sol} = \frac{1}{C_1}\ln\frac{(T_m - T_\infty)}{(T_{sol} - T_\infty)} \quad (17)$$

$$\text{where } C_1 \equiv \frac{k_v}{\delta}\frac{1}{\rho_m \Delta_m C_m}$$

and where Δ_m is the thickness of the melt. When Eq. 17 is combined with Eq. 14, integration over the time to solidification for iron oxide ($T_{sol} \cong 1800$ K) gives

$$N_H = \frac{2A}{3}\left(\frac{D_H}{R_o T_v}\right)\frac{\Delta P_H}{\delta}\left[\frac{2T_\infty + T_m(1 - C_1 t_{sol})}{T_\infty + T_m}\right]^{3/2} x\left(\frac{T_m + T_\infty}{\Delta_m C_1}\right) \quad (18)$$

Practically, once the metal oxide has begun to solidify, the rate of hydrogen generation will be reduced substantially, and Eq. 8 will predict the total amount of hydrogen produced. Table 2 gives the results when this model is applied to experiments FITS-3C and 5C, where no steam explosions occurred. Again the agreement is quite good, suggesting one can use it for experimental analysis.

Conclusions

Recent FITS-C experiments, using iron-alumina or corium A + R melt simulants, have shown that substantial amounts of hydrogen can be generated during a CMCI; when the interaction was explosive, the percentage of metal that reacted to produce hydrogen was roughly five times greater than in the non-explosive case. Predictions for the amounts of hydrogen generated using a simple model were in reasonable agreement with the experimental results.

References

1. L. D. Buxton, Molten Core-Water Contact Analysis, SAND77-1842, Sandia National Laboratories (1979).
2. W. B. Murfin, Editor, Report of the Zion/Indian Point Study: Volume 1, SAND80-0617/1, NUREG/CR-1410, Sandia National Laboratories (1980).
3. J. F. Meyer et al., Preliminary Assessment of Core Melt Accidents at the Zion and Indian Point Nuclear Power Plants and Strategies for Mitigating Their Effects, NUREG-0850, Vol. 1, USNRC Report (1981).
4. G. Klopp et al., Zion Probabilistic Safety Study, Commonwealth Edison Co. (1981).
5. R. E. Henry et al., "Establishment of a Permanently Coolable State," Trans. Am. Nucl. Soc., 39, 368 (1981).

6. L. Baker and L. C. Just, Studies of Metal-Water Reactions at High Temperatures, III Experimental and Theoretical Studies of the Zirconium-Water Reaction, ANL-6548, Argonne National Laboratory (May 1962).

7. J. V. Cathcart et al., Zirconium Metal-Water Oxidation Kinetics IV. Reaction Rate Studies, ORNL/NUREG-17, Oak Ridge National Laboratory (August 1977).

8. D. E. Mitchell, M. L. Corradini and W. W. Tarbell, Intermediate Scale Steam Explosion Phenomena: Experiments and Analysis, SAND81-0124, Sandia National Laboratories (1981).

9. M. Berman, Light Water REactor Safety Research Program Semiannual Report, October 1981 - March 1982, SAND82-1672, NUREG/CR2841, to be published.

10. B. W. Spencer et al., "Results of Scoping Tests on Corium-Water Thermal Interactions in an Ex-Vessel Geometry," 21st ASME NHTC, Seattle (July 1983).

11. M. L. Corradini, "A Proposed Model of Fuel-Coolant Mixing," Proceedings of the ANS/ENS Int'l. Mtg. on Thermal Reactor Safety, Chicago (August 1982).

12. M. L. Corradini, "Hydrogen Generation During Molten Fuel-Coolant Mixing," Proceedings of the NAS/ENS 2nd Int'l. Mtg. on Nuclear Reactor Thermal Hydraulics, Santa Barbara (January 1983).

13. M. L. Corradini and G. A. Moses, "A Dynamic Model for Fuel-Coolant Mixing," Proc. Int. Meeting on Light-Water Reactor Severe Accident Evaluation, Cambridge, MA (August - September 1983).